Available online at www.sciencedirect.com
ScienceDirect
Journal of Sound and Vibration 304 (2007) 541–555
JOURNAL OF SOUND AND VIBRATION
www.elsevier.com/locate/jsvi

Experiments on chaotic vibrations of a post-buckled beam with an axial elastic constraint

K. Nagai[a,*], S. Maruyama[a], K. Sakaimoto[b], T. Yamaguchi[a]

[a]*Department of Mechanical System Engineering, Gunma University, 1-5-1, Tenjin-cho, Kiryu, Gunma 376-8515, Japan*
[b]*Fuji Heavy Industries Ltd., 1-1, Subaru-cho, Ota, Gunma 373-8555, Japan*

Received 30 October 2005; received in revised form 12 July 2006; accepted 2 March 2007

Abstract

To clarify chaotic behavior of thin walled beams, detailed experimental results are presented on chaotic vibrations of a post-buckled beam subjected to periodic lateral acceleration. A thin steel beam of thickness 0.198 mm, breadth 12.7 mm and length 106 mm is used as a test beam. Both ends of the beam are clamped for deflection. One end of the beam is elastically constrained by an axial spring. The beam is compressed to the post-buckled configuration by the axial spring. First, characteristics of restoring force and natural frequency of the beam are obtained. Dynamic nonlinear responses of the beam are measured under periodic acceleration. In specific frequency regions, chaotic responses are generated. The chaotic responses are examined carefully with the Poincaré maps, the Fourier spectra, the maximum Lyapunov exponents and the principal component analysis.The post-buckled beam shows the soften-and-hardening characteristics of restoring force. The dominant chaotic responses of the beam are bifurcated from the sub-harmonic resonances of $\frac{1}{2}$ and $\frac{1}{3}$ orders with the lowest mode of vibration. Changing the exciting frequency gradually, dynamical transition behaviors from these steady-state sub-harmonic response to the chaotic responses are precisely inspected by the Poincaré projection. The maximum Lyapunov exponent of the former chaotic response of $\frac{1}{2}$ order is larger than that of the latter chaotic response of $\frac{1}{3}$ order. The principal component analysis predicts that the contribution of the lowest mode of vibration to the chaos is dominant among other contributions of multiple vibration modes.

1. Introduction

Thin walled structures are used in many light weight vehicles, such as spacecraft, aircraft, automobiles and railway vehicles. The thin structures are subjected to static external force and dynamic force under severe operational conditions. Furthermore, it is required to reduce the total weight of the thin structures without losing the rigidity of the structures. Beams and arches are used as fundamental elements of the thin structures. These are usually connected to other elastic elements at their boundaries. As the external forces are loaded on the elements, each element is deformed laterally and axially by an axial elastic constraint at the boundary. When the beam is compressed intensely by the axial elastic constraint, elastic buckling occurs easily in the

*Corresponding author. Tel.: +81 277 30 1584; fax: +81 277 30 1599.
E-mail addresses: nagai@eng.gunma-u.ac.jp (K. Nagai), maruyama@me.gunma-u.ac.jp (S. Maruyama), yamagme4@me.gunma-u.ac.jp (T. Yamaguchi).

0022-460X/$ - see front matter © 2007 Elsevier Ltd. All rights reserved.
doi:10.1016/j.jsv.2007.03.034

beam. Then the beam is deformed to a curved configuration in a post-buckled state. As the post-buckled beam has a sufficient curvature, the beam has higher bending rigidity than that of a straight beam. However, snap-through buckling of the post-buckled beam occurs under critical lateral force. Under periodic lateral force, a large amplitude vibration of the beam is excited by nonlinear resonance even though the amplitude of the periodic force is small. In typical frequency ranges of the periodic force, chaotic vibrations are generated. Since lateral response of the beam has nonlinear coupling with axial displacement, the generation of the chaos is drastically influenced by the small fluctuations of the axial elastic constraint. Furthermore, the chaotic response of the beam shows a violent movement due to dynamic snap-through transitions. Therefore, multiple modes of vibration are generated simultaneously in the chaotic response. It is of great importance to determine more precisely the generation of the chaotic response and the contribution of vibration modes to the chaotic response in the post-buckled beam with the axial elastic constraint.

Nonlinear vibrations and chaotic phenomena of beams and arches were investigated by many researchers including the authors. Nonlinear vibrations of a buckled beam clamped at both ends were studied by Tseng and Dugundji [1] and Yamaki et al. [2,3]. In their reports, irregular dynamic snap-through responses of the buckled beam were mentioned. Chaotic vibrations of a cantilevered buckled beam with two-well potential function were studied by Holmes [4] and Moon and Holmes [5]. Pzeshki and Dowell [6] investigated chaotic responses of a buckled beam using the Lyapunov dimension to estimate the number of vibration modes in the chaos. Azeez and Vakakis [7] introduced the principal component analysis to estimate contributions of vibration modes in the vibro-impact problem of a cantilevered beam. The authors have investigated the nonlinear vibrations of an arch [8,9] and chaotic vibrations of a post-buckled beam [10–12] both experimentally and analytically. Both ends of the arches and beams were clamped for deflection and the axial displacement was completely fixed at the boundary. In the experiments, the axial displacement was kept constant by the control on the thermal elongations of the beam and arch to that of the fixture. Chaotic phenomena of an arch [13] and a beam [14,15] with variable cross section were analyzed theoretically. Multiple-degree-of-freedom system on the beam and arch was introduced in the analyses. It was found that predominant chaotic responses are dominated by the sub-harmonic resonance responses of $\frac{1}{2}$ order and $\frac{1}{3}$ order with the fundamental mode of vibration. However, it was difficult to detect the axial displacements of the arches and the beams directly. The chaotic responses were tremendously sensitive to the axial displacement. To overcome these difficulties, first the authors analyzed the chaotic vibration of clamped arches constrained by an axial elastic support theoretically [16]. Furthermore, the authors conducted the experiment of a post-buckled reinforced beam constrained by an axial spring at the boundary [17]. Movements of the reinforced beam was restricted to that of a discrete two-link system. Responses of the reinforced beam showed basic features of chaos in a lower degree-of-freedom system. In contrast, when the chaotic responses of a post-buckled beam are generated, multiple modes of vibration contribute to the chaos simultaneously.

To clarify whole features of chaotic phenomena of a post-buckled beam elastically constrained in the axial direction, experimental results are presented precisely. In the experiment, both ends of the beam are clamped. One end of the beam is connected to an axial spring and is movable in the axial direction. The beam is compressed by an initial axial displacement through the axial spring, then the beam is deformed to a post-buckled configuration. Under periodic acceleration, chaotic responses of the beam are examined with the frequency response curves, the Fourier spectra, the Poincaré projections and the maximum Lyapunov exponents. Furthermore, under sweeping exciting frequency with a very slow rate, bifurcation behaviors from periodic responses to the chaotic response are precisely inspected by the Poincaré projection. Finally, applying the principal component analysis, that is also called as the Karhnen–Loève method [18] or the proper orthogonal decomposition, contributions of multiple modes of vibration to the chaotic response are analyzed with the time responses at multiple positions of the beam.

2. Test beam and fixture

A thin steel beam with thickness $h = 0.198$ mm, breadth $b = 12.7$ mm and length 141 mm is clamped at the both ends. The actual length of the clamped beam is $L = 106$ mm. To detect lateral displacement of the beam by a laser displacement sensor, both surfaces of the beam are painted white as a reflection target. Material properties of the beam are measured as the Young's modulus $E = 196$ GPa and the mean mass density

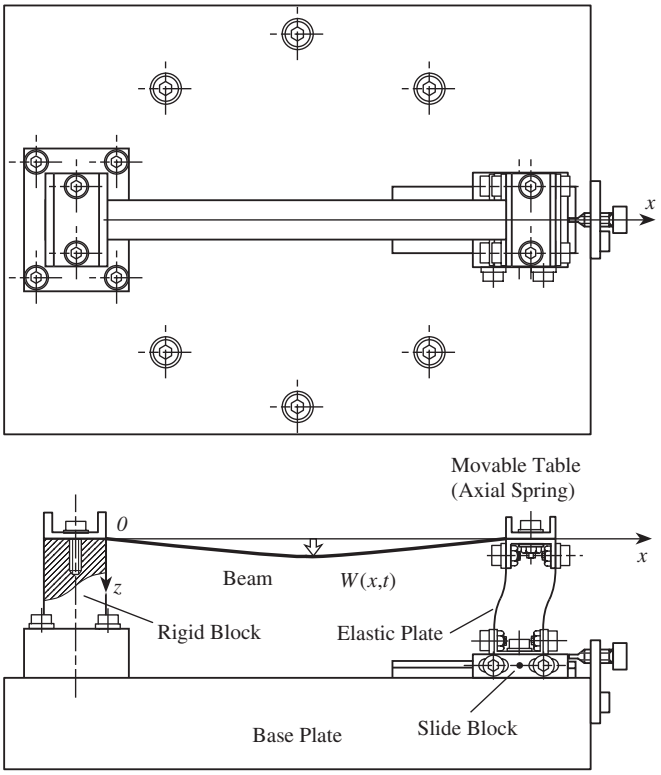

Fig. 1. Fixture of the beam and the axial elastic-constraint.

$\rho = 7.78 \times 10^3\,\mathrm{kg/m^3}$. The total mass of the beam is $m = 2.33 \times 10^{-3}\,\mathrm{kg}$. Fig. 1 shows the beam and its fixture. The fixture consists of two fixing devices of the beam ends. One end of the beam is firmly fixed to a base plate through a rigid block. The other clamped end of the beam is connected to a movable table. The movable table consists of two elastic plates on a slide block and works as the axial spring. Consequently, the beam is clamped at both the ends laterally and is elastically constrained to the axial direction. When the slide block on the base plate is compressed inward by a screw, compressive axial force is loaded on the beam. The axial force can be detected by strain gauges glued on the elastic plate. The axial spring-constant of the movable table without the beam is $K = 36.9 \times 10^3\,\mathrm{N/m}$. The lowest natural frequency of the movable table without the clamped beam is 215 Hz and an equivalent mass is calculated as $M = 28.4 \times 10^{-3}\,\mathrm{kg}$. As shown in the figure, the coordinate system is denoted by x-axis and z-axis, where the direction of z-axis corresponds to the direction of gravity. The lateral deflection of the beam is denoted by $W(x, t)$, where t is the time. As the beam is compressed by the axial spring and the axial force exceeds the critical force of buckling, the beam shows post-buckled configuration.

3. Vibration test apparatus

The post-buckled beam is excited under periodic acceleration with a system of an electromagnetic exciter through the fixture. Dynamic responses of the beam at several positions are measured with a set of multiple laser displacement sensors. A schematic diagram of the test setup is shown in Fig. 2. In the figure, devices numbered from 1 to 4 compose the set of the electromagnetic exciter. The exciter controller 1 generates a periodic sinusoidal signal which is amplified by the power amplifier 2. The vibration exciter 3 drives the fixture with periodic acceleration on which the post-buckled beam is fixed. The accelerometer 4 picks up the signal of the periodic acceleration. The signal is fed back to the exciter controller 1. Then, the peak acceleration is kept at a prescribed constant level. The electromagnetic exciter has the maximum amplitude of periodic force 1780 N. The total mass of the beam and the fixture including the moving element of the exciter is 7.4 kg, then

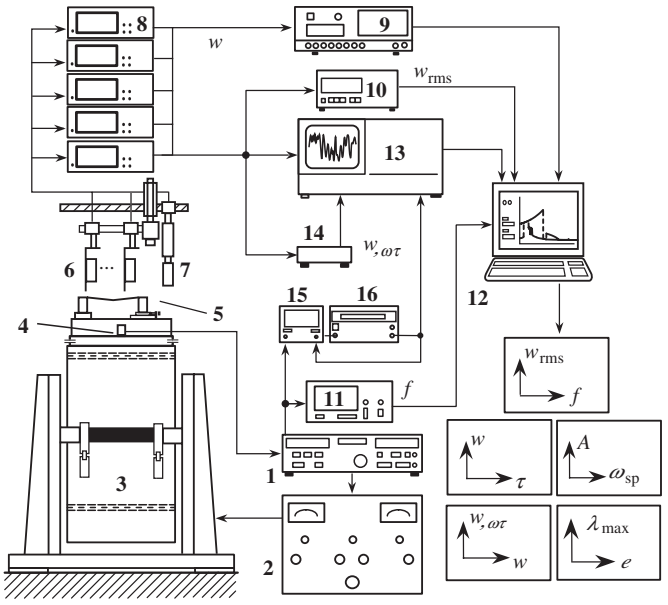

Fig. 2. Vibration test apparatus of the beam.

the maximum peak amplitude of acceleration 240 m/s^2 can be applied on the beam. The exciting frequency can be swept from 20 Hz to 10 kHz with the resolution 1.2 mHz. The lowest sweep rate is 1 mHz/s. The excitation is provided by the devices of Brüel and Kjaer products (Exciter controller: B&K 1050, Power amplifier: B&K 2078, Vibration exciter: B&K 4802 and 4818, Acceleration pickup: B&K 4371). The beam is subjected to the gravitational acceleration g and the periodic acceleration $a_d \cos 2\pi ft$, where f is the exciting frequency and a_d is the peak amplitude of acceleration.

The instruments of laser displacement sensor are numbered from 6 to 8 (Keyence LC2400, with measuring range ±3 mm). The sensor 6 detects total displacements both of the beam and the base plate of the fixture, while the sensor 7 measures the displacement of the base plate only. The controller 8 subtracts these signals, then relative displacement of the beam to the base plate is detected. To inspect contributions of multiple modes to the chaos, chaotic responses are detected simultaneously at five positions along the beam. The multi-channel digital recorder 9 (Teac DR-M2a, 8ch) acquires the dynamic responses. The digital voltmeter 10 (Advantest TR6841) transforms the response of the beam to the root mean square value. The frequency counter 11 (Advantest TR5822) measures the frequency of the periodic excitation. Then, frequency response curves of the beam are monitored by the computer 12. The digital spectrum analyzer 13 (Advantest TR9405) transforms the dynamic response to the Fourier spectrum. The Poincaré projection of the chaotic response is recorded as follows: the displacement of the chaotic response is differentiated to the velocity by the differential amplifier 14. The phase meter 15 (B&K 2971) detects the maximum point of the periodic acceleration of the excitation and then the pulse oscillator 16 (NF Elec. Instr. 1930) sends a timing signal to the analyzer 13 with a prescribed phase shift. Then, the analyzer captures both the aforementioned displacement and velocity of the chaotic response. Finally, computer 12 records the Poincaré projection of the chaos.

4. Test procedure

4.1. Non-dimensional notations

To discuss the results of the experiments, the following non-dimensional notations are introduced:

$$\xi = x/L, \quad w = W/h, \quad n_x = N_x L^2/EI, \quad [p_s, p_d] = [g, a_d]\rho AL^4/EIr,$$
$$q_s = Q_s L^3/EIr, \quad \tau = \Omega_0 t, \quad \omega = 2\pi f/\Omega_0, \tag{1}$$

where $r = \sqrt{I/A}$ represents the radius of gyration of cross section of the beam, $\Omega_0 = L^{-2}\sqrt{EI/\rho A}$ is the coefficient corresponding to lateral vibration of the beam. In Eq. (1), ξ is the non-dimensional coordinate, w is the lateral displacement normalized by the beam thickness h. Notation n_x is the non-dimensional axial force where N_x represents the axial force on the cross section. Notations p_s and p_d are the non-dimensional force intensities related to the gravitational acceleration g and the peak acceleration of periodic excitation a_d, respectively. When the characteristics of restoring force of the beam is examined, static lateral deflection by the concentrated static force Q_s is measured. Notation q_s is the non-dimensional static force. Notations ω and τ are the non-dimensional exciting frequency and the time, respectively. Non-dimensional exciting force is expressed as $p_s + p_d \cos\omega\tau$.

4.2. Fundamental properties of the post-buckled beam

To find fundamental properties of the post-buckled beam, the linear natural frequencies and the restoring force are inspected.

Applying periodic acoustical pressure and impact force on the beam, linear natural frequencies of lateral vibration and of longitudinal vibration, respectively, are detected with the spectrum analyzer. The lowest natural frequency of the beam is measured by increasing the axial compressive force. Fig. 3 shows the lowest linear natural frequency ω_1 of the beam under the axial compressive force $-n_x$. The static lateral force p_s loaded initially on the beam is $p_s = 271$ by the gravitational acceleration ($g = 9.798\,\mathrm{m/s^2}$). The actual lowest natural frequency f_1 measured with Hz is also indicated on the abscissa. Increasing the compressive force from $n_x = 0$, the frequency ω_1 decreases gradually. When the natural frequency $\omega_1 = 12.7$ takes a minimum finite value, the axial force corresponds to the critical compressive force $n_{\mathrm{cr}} = -36.0$ ($N_{\mathrm{cr}} = -5.16\,\mathrm{N}$) of the buckling. The finite value of the frequency is due to the static deflections by the gravity force and inevitable initial imperfection. The initial imperfection of the beam appears inherently during the fabrication of the beam. The initial imperfection involves an initial deflection and deformation caused by the clamp at the ends. Further, the axial force is increased more than the critical force n_{cr}, the natural frequency ω_1 increases steeply. The reason of the steep increment of the frequency is explained as follows: as the post-buckled deflection of the beam increases, the stiffness of the beam increases by a geometrical nonlinear relation with deflection and axial displacement.

Fixing the beam to the post-buckled form with the axial force $n_x = -40.9$ ($N_x = -5.86\,\mathrm{N}$), which corresponds to 1.14 times of the critical force, the natural frequencies are found to be $\omega_1 = 19.5$ ($f_1 = 78.0\,\mathrm{Hz}$), $\omega_2 = 44.3$ ($f_2 = 177\,\mathrm{Hz}$) and $\omega_3 = 99.8$ ($f_3 = 399\,\mathrm{Hz}$). Where ω_1, ω_2 and ω_3 correspond to the lowest, the second and the third modes of lateral vibration, respectively. An axial vibration is excited by an impact hammer. The natural frequency of axial vibration is measured by the Fourier analyzer. The natural frequency of axial vibration of the beam is 9.4 times greater than the natural frequency ω_1 of the lowest mode of lateral vibration.

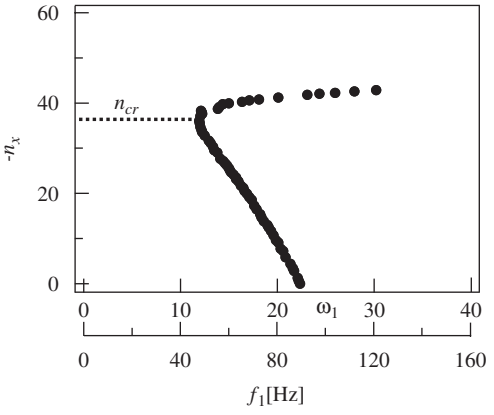

Fig. 3. Natural frequency of the beam under axial compression, n_{cr} is the critical force of the buckling.

Furthermore, to obtain the characteristics of restoring force, the relation between static lateral deflection w and static concentrated force q_s is measured with a laser displacement sensor and a load cell. The load cell consists of a dual-cantilevered beam with a tip needle. A strain gauge is glued on the cantilevered beam. Pressing the load cell to the buckled beam through the tip needle, the buckled beam shifts to an equilibrium position of elastic force between the beam and the load cell. The intensity of the concentrated force is detected with the strain gauge, while the deflection of the buckled beam is measured with the laser sensor. Under the axial force $n_x = -40.9$ and the gravitational force $p_s = 271$, the static deflection at the mid point of the beam shows 12.5 times of the beam thickness (the actual static deflection is 2.48 mm). Fig. 4 shows the static lateral deflection w at the position $\xi = 0.3$ under the concentrated force q_s loaded on the mid span of the beam. The origin of deflection is selected at the static equilibrium position of the beam under the axial compressive force and the gravity. The characteristics of restoring force of the post-buckled beam show the type of a softening-and-hardening spring including a negative gradient. In the figure, the deflection of the beam changes from $w = -12$ ($W = -2.4$ mm) to $w = 4$ ($W = 0.79$ mm), while the concentrated force q_s covers from $q_s = -6000$ ($Q_s = -0.44$ N) to $q_s = 6000$ ($Q_s = 0.44$ N). When the force increases to the negative z-direction (upward against the gravity), the beam deflects showing the characteristics of a softening spring from $w = 0$ to the negative direction. As the deflection is close to $w = -2.46$, the magnitude of the force q_s saturates. In the range of deflection from $w = -2.46$ to -7.23, the restoring force shows a negative gradient. As the deflection increases more than $w = -7.23$, the restoring force turns to the type of a hardening spring. In addition, without the concentrated force, the post-buckled beam has two stable equilibrium positions, at $w = 0$ and -8.2.

4.3. Test procedure of chaotic vibration

Applying the periodic excitation $p_s + p_d \cos \omega\tau$ on the post-buckled beam, chaotic responses of the beam are investigated. Under the non-dimensional static force $p_s = 271$, the peak amplitude of periodic excitation $p_d = 1174$ ($a_d = 40\,\mathrm{m/s^2}$) is selected. To find frequency regions where chaotic responses are generated, the nonlinear frequency response curves are inspected. The exciting frequency is changed slowly within the range from $\omega = 10$ ($f = 40$ Hz) to $\omega = 50$ ($f = 200$ Hz) with the sweep rate of the frequency 0.1 Hz/s. The instability boundaries of the chaotic response are obtained by changing the amplitude of the periodic exciting force from $p_d = 500$ ($a_d = 17.0\,\mathrm{m/s^2}$) to $p_d = 1470$ ($a_d = 50.0\,\mathrm{m/s^2}$) and by changing the exciting frequency. Time responses of the chaotic vibrations are examined with the Fourier spectra, the Poincaré projections and the maximum Lyapunov exponents. Bifurcation phenomena from the periodic response to the chaotic response are inspected with the Poincaré projection for the response of deflection by the continuous change of the exciting frequency. The maximum Lyapunov exponent $\lambda_{\max}$ of the chaotic response is calculated with the procedure by Wolf et al. [19] and Takens [20]. Increasing the embedding dimension e in the pseudo phase space, if the maximum Lyapunov exponent $\lambda_{\max}$ is saturated to a constant value, the maximum Lyapunov exponent $\lambda_{\max}$ and the embedding dimension e of the inspected response are determined. If the $\lambda_{\max}$ takes a

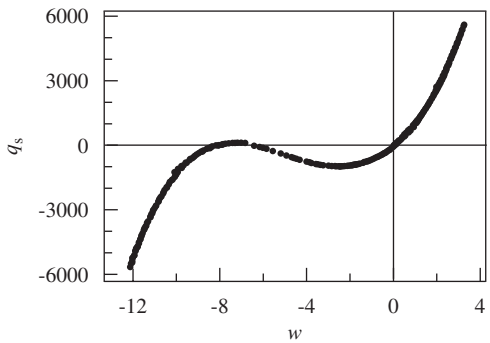

Fig. 4. Characteristics of the restoring force under concentrated load q_s at $\xi = 0.5$, measurement point is $\xi = 0.3$, $n_x = 40.9(= 1.14n_{\mathrm{cr}})$.

positive value, the response is confirmed as the chaos. Half of the embedding dimension corresponds to the number of vibration modes which predominantly contribute to the chaotic response [6].

Finally, measuring simultaneous responses at multiple positions of the post-buckled beam, the principal components are calculated by the Karhunen–Loève transformation [7,18,21]. The K–L transformation enables one to estimate contribution ratio and related modal pattern in the chaotic response of the post-buckled beam. Results of the principal component analysis cannot strictly predict the nonlinear modes of vibration. However, the principal component analysis represents an optimal estimation of linear modes to the nonlinear time responses.

5. Results and discussion

5.1. Frequency response curves of the post-buckled beam

Nonlinear response curves of the post-buckled beam are obtained under the static force and the periodic exciting force $p_s + p_d \cos\omega\tau$. The results are shown in Fig. 5 under the non-dimensional force amplitude of excitation $p_d = 1174$. The ordinate w_{rms} indicates the root mean square value of the dynamic response at the position $\xi = 0.3$ of the beam, while the abscissa ω denotes the non-dimensional exciting frequency. The actual exciting frequency f measured with Hz is also indicated on the abscissa. Notation $(i : j)$ denotes the type of resonance, in which index i is a generated mode of vibration, while index j denotes a type of resonance. For example, $j = 1$ indicates the principal resonance, while $j = \frac{1}{3}$ is the sub-harmonic resonance of $\frac{1}{3}$ order. The chaotic response is represented by the notation $\mathrm{C}(i : j)$, in which indices i and j correspond to the dominant mode of vibration and the type of resonance, respectively. Natural frequencies of the post-buckled beam are also indicated by the solid circles on the abscissa.

In the figure, the nonlinear response curve corresponds to the characteristics of restoring force with the type of a softening-and-hardening spring. Decreasing the exciting frequency ω from upper region, first, the principal resonance response (2:1) is generated with the second mode of vibration at the frequency $\omega = 44.0$. As the frequency is decreased, the sub-harmonic resonance response $(1 : 1/2)$ is bifurcated from the non-resonant response at $\omega = 36.8$. The amplitude increases as the exciting frequency decreases. The behavior of the response corresponds to the characteristics of restoring force of a softening spring within the smaller amplitude. The amplitude of the sub-harmonic resonance transits to the non-resonant response by a jump phenomenon at $\omega = 28.3$. Furthermore, decreasing the exciting frequency ω, two types of chaotic responses are observed clearly. The chaotic responses are generated first from the non-resonant response with the jump phenomenon. As will be shown later in Figs. 13 and 14, the maximum Lyapunov exponents of these responses have positive values, then the responses are confirmed as the chaos. Moreover, these chaotic responses are significantly dominated by the sub-harmonic resonance response with the type of a softening-and-hardening spring. In the higher frequency range from $\omega = 18.3$ to 17.6, the chaotic response $\mathrm{C}(1 : 1/3)$ is dominated

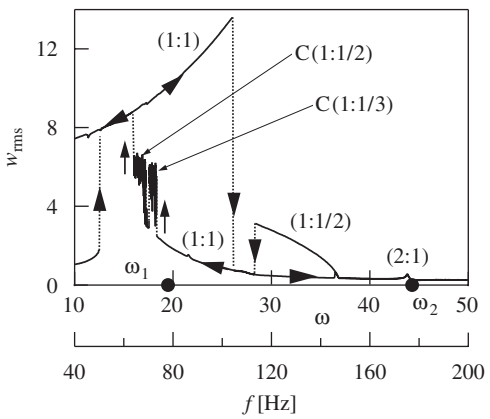

Fig. 5. Frequency response curve, $p_d = 1174$, $\xi = 0.3$, sweep rate = 0.1[Hz/s].

predominantly by the sub-harmonic resonance response of $\frac{1}{3}$ order accompanied with the lowest mode of vibration. In the lower range from $\omega = 17.3$ to 16.1, the chaotic response C(1 : 1/2) appears corresponding to the sub-harmonic resonance response of $\frac{1}{2}$ order. These chaotic responses are generated with larger amplitude in the lower frequency regions than the higher frequency regions where the corresponding sub-harmonic resonance in smaller amplitude is generated. However, the maximum amplitudes in these chaotic responses are less than the large amplitude of the principal resonance with the lowest vibration mode. When the exciting frequency decreases to $\omega = 16.1$, the chaotic response C(1 : 1/2) transits to the response of the principal resonance. The principal resonance shows the response corresponding to a hardening spring.

5.2. Instability boundaries of the chaotic vibration

Changing the amplitude of periodic force p_d and the exciting frequency ω, instability boundaries are obtained where the chaotic responses are generated. Under different magnitudes of the amplitude p_d, the frequency response curves of the chaotic responses are shown in Fig. 6. When the excitation amplitude increases as (a) $p_d = 625$, (b) $p_d = 898$, (c) $p_d = 1174$ and (d) $p_d = 1460$, the instability region of the chaos separates into two groups. The instability regions are shown in Fig. 7. When the amplitude p_d is small, chaotic response is not generated. As the amplitude p_d increases to the magnitude of $p_d = 630$, the chaotic response C(1 : 1/2) due to the sub-harmonic resonance of $\frac{1}{2}$ order appears first. More than large amplitude $p_d = 1077$, the chaotic response C(1 : 1/3) is also generated. These chaotic regions are shifted proportionally to the higher frequency range as the exciting amplitude p_d increases.

5.3. Time progresses, Fourier spectra and Poincaré projections of the chaotic responses

The nonlinear time progresses approaching the chaotic responses C(1 : 1/3) and C(1 : 1/2) are examined by the Fourier spectra and the Poincaré projections. The nonlinear progresses are measured at the point $\xi = 0.3$ of the beam under the amplitude of periodic force $p_d = 1174$. In the frequency range including the chaotic response C(1 : 1/3), the results at the exciting frequencies $\omega = 18.28, 18.08$ and 17.98 are shown in Fig. 8(a)–(c), respectively. In the left-side figures, the time progresses of the non-dimensional deflection w are shown by the time scale of excitation period τ_e. The Fourier spectra of these responses are presented in the middle figures. In the figure, the ordinate stands for the Fourier amplitude A of which level is scaled with decibel, while the abscissa indicates the non-dimensional frequency of spectrum ω_{sp} with logarithmic scale. The right-hand-side figures are the Poincaré projections. The deflection w and the velocity $w_{,\omega\tau}$ at the position $\xi = 0.3$ of the beam are recorded in every period of the excitation. In the projections, 6000 points are plotted on the phase plane with the delay of phase $\theta = -2\pi/3$ from the maximum amplitude of the exciting force. In Fig. 8(a), the time progress at the frequency $\omega = 18.28$ shows an almost periodic response. The small

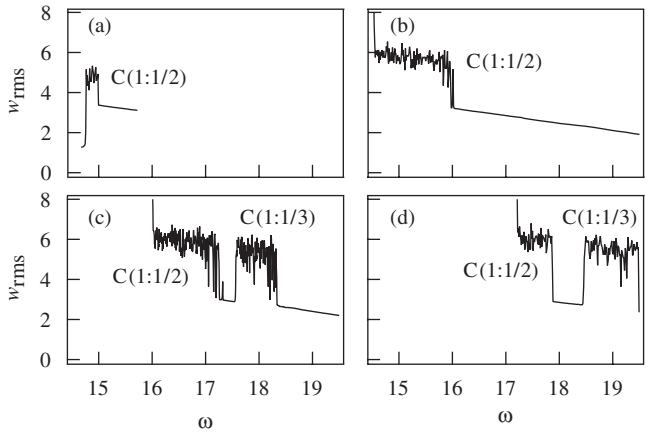

Fig. 6. Frequency response of chaotic responses, (a) $p_d = 625$; (b) $p_d = 898$; (c) $p_d = 1174$; (d) $p_d = 1460$.

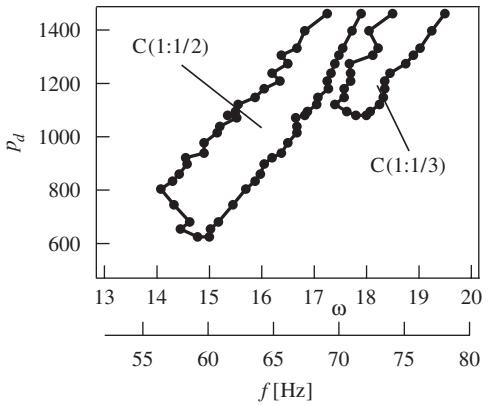

Fig. 7. Instability boundaries of the chaos.

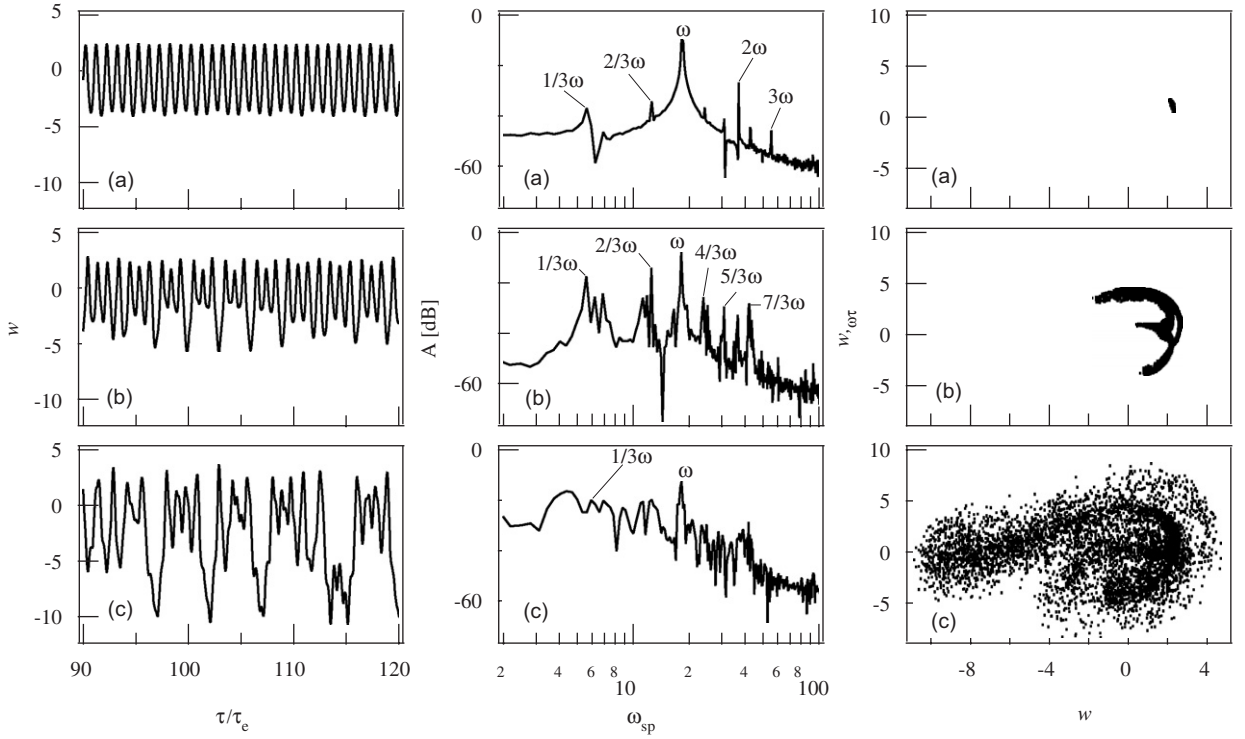

Fig. 8. Time progresses, Fourier spectra and Poincaré projections of the responses of the beam C(1 : 1/3), (a) $\omega = 18.28$; (b) $\omega = 18.08$; (c) $\omega = 17.98$.

amplitude response corresponds to the non-resonant vibration around the position $w = 0$, i.e., the one of the static equilibrium points. The dominant spike of the Fourier spectrum indicates the fundamental harmonics of the excitation. Other spikes appear at the frequency related to the sub-harmonic component of $\frac{1}{3}$ order and the higher harmonic components of the exciting frequency. The Poincaré projection of the almost periodic response shows the concentrated figure of attractor. As the frequency is decreased to $\omega = 18.08$, the time progress in Fig. 8(b) indicates irregular amplitude modulation. The time progress involves the response of the sub-harmonic component of $\frac{1}{3}$ order among the periodic response of the excitation. The Fourier spectrum has the distinct sub-harmonic components of orders $i/3$ $(i = 1, 2, 3, 4, 5, \ldots)$. The related Poincaré projection shows the condensed closed loop with three sharp bends in the phase plane. The figure of the attractor

represents the response of the sub-harmonic resonance of $\frac{1}{3}$ order with the amplitude modulation. When the frequency is changed to $\omega = 17.98$, the chaotic response of the type C(1 : 1/3) appears drastically. In the large amplitude chaotic response the beam transits irregularly between the two stable equilibrium points, $w = 0$ and -8.2, involving dynamic snap-through. However, the time response around $w = -8.2$ does not appear compared with the time response around $w = 0$. The Fourier spectrum of the chaotic response has lump spectrum around one-third of the exciting frequency ω. Therefore, the chaotic response C(1 : 1/3) is generated from the predominant response of the sub-harmonic resonance of $\frac{1}{3}$ order. The Poincaré projection of the chaotic response of the type C(1 : 1/3) spreads out to a scattered figure, involving the figure of three sharp bends. A fractal pattern is clearly constructed in this Poincaré projection. Fig. 9 shows the variation of the Poincaré projections for the chaotic response C(1 : 1/3) at the exciting frequency $\omega = 17.8$, changing the phase delay θ with the increment of $\pi/3$ rad. As the phase angle is shifted, the projection rotates clockwise accompanied by folding-and-stretching in the fractal figure.

Fig. 10 shows the time progress, the corresponding Fourier spectra and the Poincaré projections of the responses including the chaotic response C(1 : 1/2) in the frequency region from $\omega = 17.48$ to 16.63. When the exciting frequency decreases from $\omega = 17.48$ to 16.78, the periodic time response around $w = 0$ increases towards the other static equilibrium point $w = -8.2$. Furthermore, the sub-harmonic components of $\frac{1}{2}$ order in the periodic response are generated. The corresponding figure of the Poincaré projection is enlarged. In the chaotic response at $\omega = 16.63$, the time progress involves both irregular responses of small amplitude and of large amplitude. The large amplitude response transits between two equilibrium points with same order of occurrence. The corresponding Fourier spectrum shows the broad-band distribution in the frequency of spectrum. The lumped spectrum of the chaotic response is distributed close to the frequency of the sub-harmonic component of $\frac{1}{2}$ order. The figure of the Poincaré projection is similar to the result of the chaos C(1 : 1/3) in Fig. 8(c). However, the projections are more condensed around the two static equilibrium points $w = -8.2$ and 0 than the projections of C(1 : 1/3). Furthermore, the figure has a different fractal pattern around the points of $w = 2$ and $w_{,\omega\tau} = 0$.

5.4. Bifurcation behavior to the chaotic responses

To confirm the bifurcation behavior from the sub-harmonic responses of $\frac{1}{3}$ order and of $\frac{1}{2}$ order to the chaotic responses, the Poincaré projections of the deflections are recorded by decreasing the exciting frequency gradually under the amplitude of periodic force $p_d = 1174$. The Poincaré projection of the chaos C(1 : 1/3) from the exciting frequency $\omega = 18.38$ to 17.75 is shown in Fig. 11. In Fig. 11(a), first, the Poincaré projection

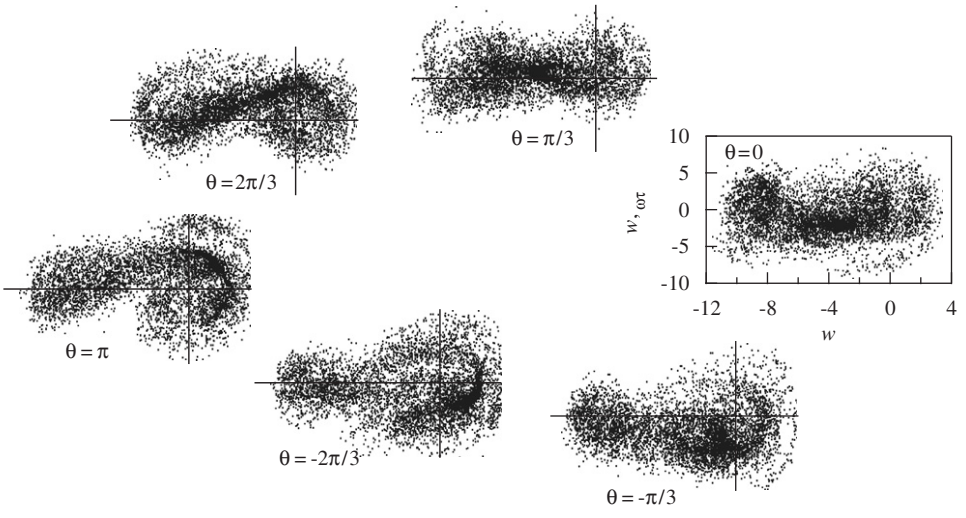

Fig. 9. Poincaré projection in each phase delay θ, C(1 : 1/3), $\omega = 17.80$.

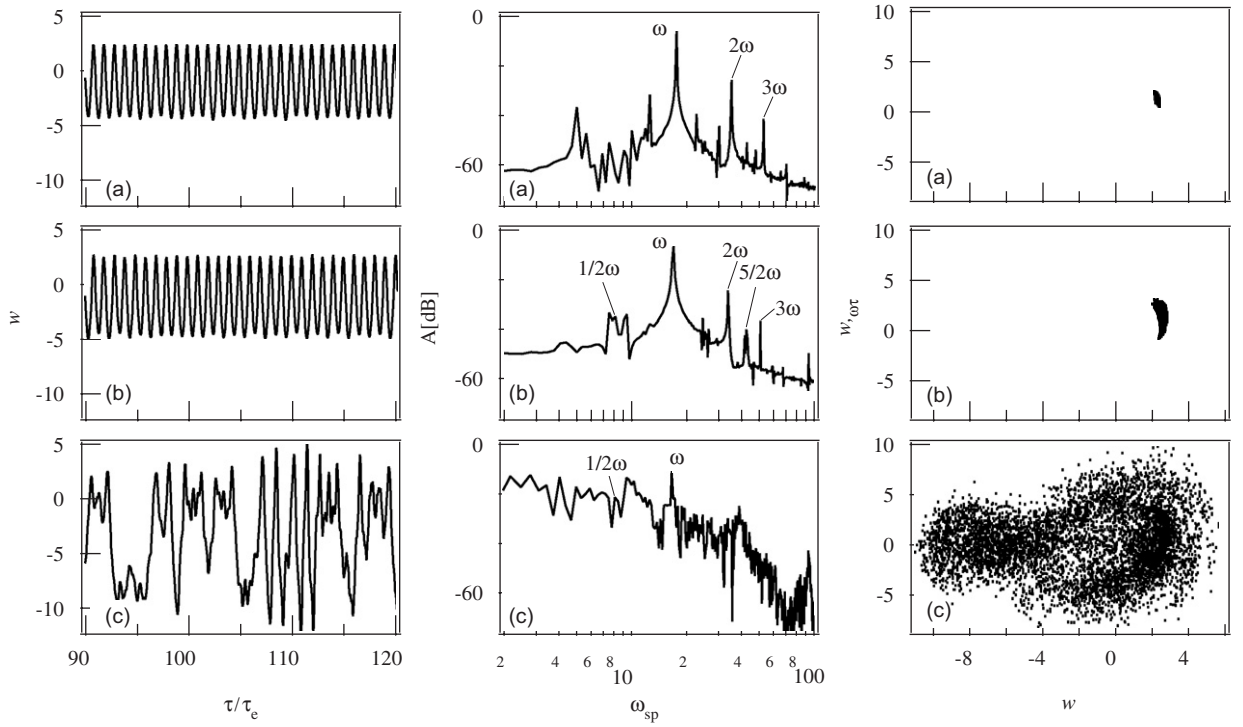

Fig. 10. Time progresses, Fourier spectra and Poincaré projections of the responses of the beam C(1 : 1/2), (a) $\omega = 17.48$; (b) $\omega = 16.78$; (c) $\omega = 16.63$.

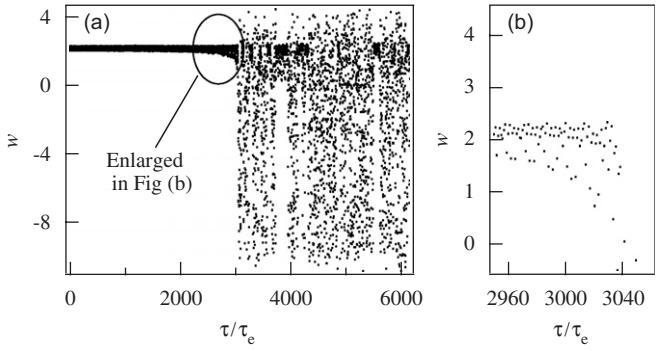

Fig. 11. Transition to the chaotic response C(1 : 1/3) from $\omega = 18.38$ to $\omega = 17.75$.

shows the steady-state periodic response of non-resonance, within the restricted amplitude. Then, the projection suddenly spreads to large amplitude and the response transits to the chaotic vibration. The projection during the transition to the chaos is enlarged in Fig. 11(b). In the figure, it is clearly observed that the points of projection construct three layers along the time sequence. Then the chaotic response is bifurcated from the sub-harmonic periodic response of $\frac{1}{3}$ order.

Fig. 12 is the time variation of the Poincaré projection in the transition to the chaos C(1 : 1/2). The exciting frequency is decreased from $\omega = 17.08$ to 16.50. In Fig. 12(a), the almost steady-state periodic response of the sub-harmonic resonance of $\frac{1}{2}$ order suddenly transits to the chaotic response. As can be seen from the enlarged Poincaré projection in Fig. 12(b), two dotted layers of the projection is also observed clearly. This implies that the chaos is bifurcated from the sub-harmonic periodic response of $\frac{1}{2}$ order. Consequently, the bifurcation behavior from the sub-harmonic responses of $\frac{1}{3}$ order and of $\frac{1}{2}$ order to the chaos is confirmed by the precise measurement in the experiment.

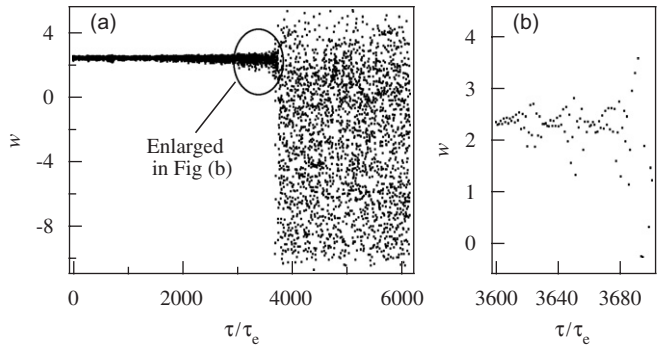

Fig. 12. Transition to the chaotic response C(1 : 1/2) from $\omega = 17.08$ to $\omega = 16.50$.

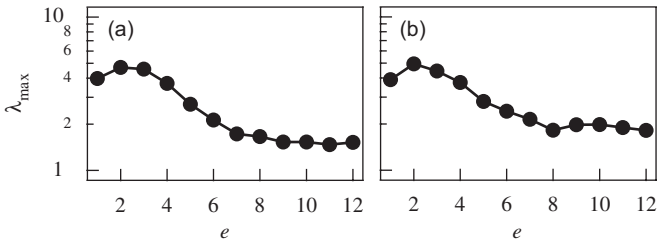

Fig. 13. Maximum Lyapunov exponent related to embedding dimension, (a) C(1 : 1/3), $\omega = 17.9$; (b) C(1 : 1/2), $\omega = 16.5$.

5.5. Maximum Lyapunov exponents of the chaotic responses

Based on the time progresses of the chaotic responses, the maximum Lyapunov exponents are calculated by the Wolf's method. Fig. 13(a) shows the maximum Lyapunov exponents λ_{max} related to the embedding dimension e of the chaotic response C(1 : 1/3) at the exciting frequency $\omega = 17.9$ under the periodic force $p_d = 1174$. As the embedding dimension e increases to $e = 7$ or 8, the maximum Lyapunov exponent λ_{max} converges to $\lambda_{max} = 1.6$. Furthermore, the result of the chaotic response C(1 : 1/2) at the frequency $\omega = 16.5$ is also shown in Fig. 13(b). The maximum Lyapunov exponent λ_{max} converges to $\lambda_{max} = 1.9$. As the maximum Lyapunov exponents converge to the positive constant values, these responses are confirmed as the chaos.

Fig. 14 shows the maximum Lyapunov exponent λ_{max} in each exciting frequency ω. The maximum Lyapunov exponents of the chaos C(1 : 1/3), in the frequency region from $\omega = 18.0$ to 17.5, take values from $\lambda_{max} = 1.1$ to $\lambda_{max} = 1.7$, and averaged value is calculated as $\lambda_{max} = 1.5$. In the region of the chaos C(1 : 1/2) from $\omega = 16.7$ to 16.4, the maximum Lyapunov exponent ranges from $\lambda_{max} = 1.3$ to 1.9, and averaged exponent takes $\lambda_{max} = 1.7$. Consequently the maximum Lyapunov exponent of the chaos C(1 : 1/2) in the lower frequency region takes larger value than that of the chaos C(1 : 1/3).

5.6. Contributions of vibration modes to the chaotic responses

The chaotic responses of C(1 : 1/3) and C(1 : 1/2) are confirmed as the chaos by the positive maximum Lyapunov exponents in Fig. 13. Furthermore, the positive maximum Lyapunov exponents converge at the embedding dimension from $e = 7$ to 8, then the number of the predominant modes of vibration which contribute to the chaos is counted as three or four.

By using the principal component analysis to the chaotic time responses at multiple positions of the post-buckled beam, contributions of vibration modes to the chaotic response are determined. The chaotic time progresses of deflection are detected simultaneously at five positions along the beam. The positions are selected as $\xi = 0.09, 0.36, 0.5, 0.64$ and 0.91. Applying the principal component analysis, contribution ratio and

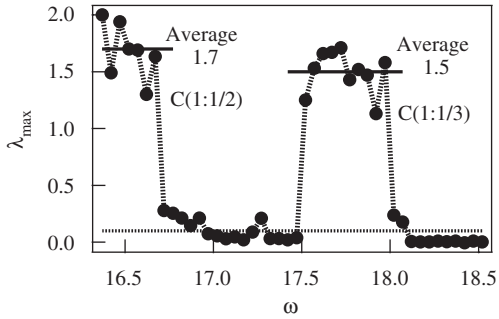

Fig. 14. Maximum Lyapunov exponent in each exciting frequency.

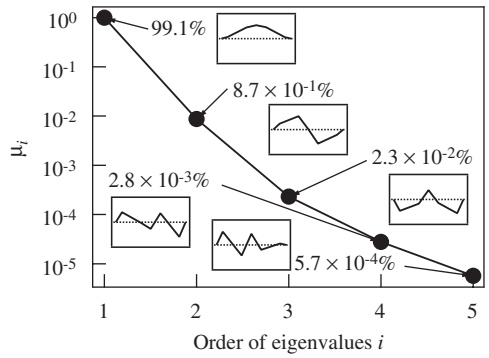

Fig. 15. Principal components in the chaotic vibration C(1 : 1/3), $\omega = 17.8$.

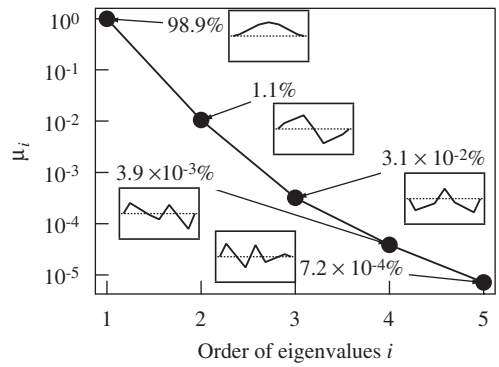

Fig. 16. Principal components in the chaotic vibration C(1 : 1/2), $\omega = 16.6$.

related modal pattern are calculated. Fig. 15 shows the contribution ratio for the chaotic response C(1 : 1/3) at the frequency $\omega = 17.8$ under the periodic force $p_d = 1174$. The ordinate denotes the contribution ratio μ_i of each principal component, while the abscissa is the order of eigenvalue i. Modal patterns are also illustrated in the figure. The largest principal component, which corresponds to the lowest vibration mode, prevails the contribution ratio of 99.1%. The contribution ratios of the second and third modes are 0.87% and 0.023%, respectively. Furthermore, the contribution ratio for the chaotic response C(1 : 1/2) at the frequency $\omega = 16.6$ is shown in Fig. 16. The largest principal component related to the lowest mode of vibration takes 98.9%. The second and the third modes have 1.1% and 0.031% of the contribution ratios, respectively.

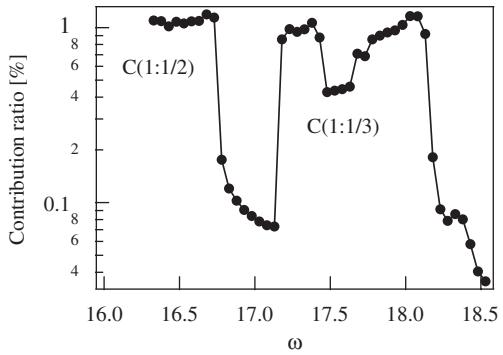

Fig. 17. Contribution ratio of higher modes of vibration to the chaos in each exciting frequency.

Changing the exciting frequency, contributions of the higher modes to the chaotic vibration are examined. Fig. 17 shows the sum of contribution ratios of the higher modes in each exciting frequency ω. In the frequency range where the chaotic responses are generated, contribution ratio of the lowest mode of vibration is more than 98%. The higher modes of vibration also contribute from 1% to 2%. Therefore, the lowest mode of vibration contributes predominantly to the chaotic response. The contribution of the higher modes of vibration to the chaotic response C(1 : 1/2) is slightly larger than that to the chaos C(1 : 1/3).

6. Conclusions

Precise experiments have been carried out on the chaotic vibrations of a post-buckled beam both ends clamped with an axial elastic constraint at one end. Chaotic responses of the post-buckled beam are inspected in detail. The main results are summarized as follows:

(1) Dominant chaotic responses of the post-buckled beam correspond to the sub-harmonic resonances of $\frac{1}{2}$ order and of $\frac{1}{3}$ order. The chaotic responses are bifurcated owing to the characteristics of restoring force with the type of a softening-and-hardening spring.
(2) The time progress and the Poincaré projections of chaotic response with the sub-harmonic resonance of $\frac{1}{2}$ order show a qualitative difference from the chaotic response with the sub-harmonic resonance of $\frac{1}{3}$ order, although these chaotic responses are generated in the neighboring frequency region. Bifurcation processes from the periodic sub-harmonic resonance responses to the chaotic responses are definitely clarified with the Poincaré projection by decreasing the exciting frequency very slowly.
(3) Under smaller amplitude of excitation, chaotic response of the sub-harmonic resonance of $\frac{1}{2}$ order is easily generated than the chaos of the sub-harmonic resonance of $\frac{1}{3}$ order. Instability boundaries of the chaotic responses are shifted to higher frequency range as the excitation amplitude increases.
(4) The maximum Lyapunov exponent of the chaos with the sub-harmonic response of $\frac{1}{2}$ order takes larger averaged value of 1.7 than the exponent 1.5 of the chaos with the sub-harmonic response of $\frac{1}{3}$ order. By the saturated maximum Lyapunov exponent to the embedding dimension, the number of the vibration modes contributed to the chaos is counted as three or four.
(5) The principal component analysis is carried out over the frequency regions of the two chaotic responses dominated by the sub-harmonic resonances of $\frac{1}{2}$ order and $\frac{1}{3}$ order. The lowest mode of vibration contributes more than 98% to the chaotic responses among other contributions of multiple vibration modes.

Acknowledgements

The authors wish to thank Mr. M. Oya and Mr. Y. Tsuruta for drafting the figures.

References

[1] W.Y. Tseng, J. Dugundji, Nonlinear vibrations of a buckled beam under harmonic excitation, *ASME Journal of Applied Mechanics* 38 (1971) 467–476.

[2] N. Yamaki, A. Mori, Non-linear vibrations of a clamped beam with initial deflection and initial axial displacement, part I: theory, *Journal of Sound and Vibration* 71 (3) (1980) 333–346.

[3] N. Yamaki, K. Otomo, A. Mori, Non-linear vibrations of a clamped beam with initial deflection and initial axial displacement, part II: experiment, *Journal of Sound and Vibration* 71 (3) (1980) 347–360.

[4] P.J. Holmes, A nonlinear oscillator with a strange attractor, *Philosophical Transactions of the Royal Society of London A* 292 (1979) 419–448.

[5] F.C. Moon, P.J. Holmes, The magnetoelastic strange attractor, *Journal of Sound and Vibration* 65 (2) (1979) 276–296.

[6] C. Pezeshki, E.H. Dowell, Generation and analysis of Lyapunov exponents for the buckled beam, *International Journal of Non-Linear Mechanics* 24 (2) (1989) 79–97.

[7] M.F.A. Azeez, A.F. Vakakis, Proper orthogonal decomposition (POD) of a class of vibroimpact oscillation, *Journal of Sound and Vibration* 240 (5) (2001) 859–889.

[8] K. Nagai, Nonlinear vibrations of a shallow arch under periodic lateral force (Theory), *Transaction of the JSME, Series C* 51 (471) (1985) 2820–2827 (in Japanese).

[9] K. Nagai, Nonlinear vibrations of a shallow arch under periodic lateral force (2nd Report, Experiment), *Transaction of the JSME, Series C* 52 (484) (1986) 3047–3054 (in Japanese).

[10] K. Nagai, Experimental study of chaotic vibration of a clamped beam subjected to periodic lateral forces, *Transaction of the JSME, Series C* 56 (525) (1990) 1171–1177 (in Japanese).

[11] K. Nagai, T. Yamaguchi, Chaotic vibrations of a post-buckled beam carrying a concentrated mass (1st Report, Experiment), *Transaction of the JSME, Series C* 60 (579) (1994) 3733–3740 (in Japanese).

[12] T. Yamaguchi, K. Nagai, Chaotic vibrations of a post-buckled beam carrying a concentrated mass (2nd Report, Theoretical analysis), *Transaction of the JSME, Series C* 60 (579) (1994) 3741–3748 (in Japanese).

[13] T. Yamaguchi, K. Nagai, Chaotic oscillations of a shallow arch with variable cross section subjected to periodic excitation, *Transaction of the JSME, Series C* 61 (583) (1995) 799–807 (in Japanese).

[14] K. Nagai, T. Yamaguchi, Chaotic vibrations of a post-buckled beam with variable cross section under periodic excitation, *Transaction of the JSME, Series C* 61 (586) (1995) 2202–2209 (in Japanese).

[15] T. Yamaguchi, K. Nagai, H. Suzuki, Interaction between internal resonance and dynamic snap-through in chaotic vibrations of a post-buckled beam with variable-cross-section, *Transaction of the JSME, Series C* 66 (652) (2000) 3820–3827 (in Japanese).

[16] K. Nagai, S. Ohyama, T. Yamaguchi, Chaotic vibrations of shallow arches with variable-cross-section constrained by an axial elastic support, *Transaction of the JSME, Series C* 64 (624) (1998) 2816–2823 (in Japanese).

[17] K. Nagai, K. Kasuga, M. Kamada, T. Yamaguchi, K. Tanifuji, Experiment on chaotic oscillations of a post-buckled reinforced beam constrained by an axial spring, *JSME International Journal, Series C* 41 (3) (1998) 563–569.

[18] M.M. Loève, *Probability Theory*, Von Nostrand, Princeton, NJ, 1955.

[19] A. Wolf, J.B. Swift, H.L. Swinney, J.A. Vastano, Determining Lyapunov exponents from a time series, *Physica* 16D (1985) 285–317.

[20] F. Takens, Detecting strange attractors in turbulence, in: D. Rand, L. Young (Eds.), *Lecture Notes in Mathematics*, Vol. 898, Springer, New York, 1981, pp. 366–381.

[21] B.F. Feeny, R. Kappagantu, On the physical interpretation of proper orthogonal modes in vibrations, *Journal of Sound and Vibration* 211 (4) (1998) 607–616.